Turbulence Measurements in Shock-Induced Flows

James W. Trolier*
Science Applications Inc., Wayne, Pennsylvania
and
Robert E. Duffy†
Rensselaer Polytechnic Institute, Troy, New York

Turbulence measurements have been made in the incident and reflected flows of a shock tube. Amplification of turbulence across the reflected shock is then determined. Hot-wire anemometers were used to measure mass flux and total temperature fluctuations. Incident flow conditions were $M = 0.47$, with $25{,}000 < Re/\text{in.} < 170{,}000$. Incident region mass flux and total temperature fluctuations averaged 1.2 and 0.5%, respectively. Reflected region conditions were nominally $M = 0.15$ and $12{,}000 < Re/\text{in.} < 85{,}000$. The reflected shock amplified the turbulence intensities by a factor of approximately 3. Turbulence amplification across a shock wave decreases, in general, with Reynolds number, over the Reynolds number range covered.

Nomenclature

A_a = dynamic sensitivity to fluctuation in adiabatic wire resistance, $a^2 - s^2\delta/[2a^2(1-\delta)]$
A_h = dynamic sensitivity to fluctuation in heat-transfer coefficient, $b^2/[2a^2(1-\delta)]$
A'_w = overheat parameter, $\frac{1}{2}\,[\partial(\ell nR_w)/\partial(\ell nI)]$
a^2 = $\alpha R_0 I^2 \ell/\pi d^2 k_w$
b^2 = $s^2 - a^2$
c,d = wire specific heat and diameter
e = anemometer bridge voltage
h = heat transfer coefficient
I = anemometer bridge current
j = $\sqrt{-1}$
k = thermal conductivity
K = $\partial(\ell nR_w)/\partial(\ell nT_w)$
ℓ,m = wire length and mass per length
M = Mach number
m_t = $\partial(\ell n\mu_w)/\partial(\ell nT_w)$
Nu = Nusselt number, hd/k_w
n_t = $\partial(\ell nk_t)/\partial(\ell nT_t)$
p = pressure
R = resistance
Re = Reynolds number, $\rho ud/\mu$
$R_{\delta\xi}$ = correlation coefficient, $\xi'\delta'/\overline{\xi\delta}$
s^2 = $h\ell^2/dk_w$
S_ρ, S_u, S_{T_t} = sensitivity of the anemometer to density, velocity, and total temperature fluctuations
T_t = total temperature
u = velocity
α = $[1 + ((\gamma-1)/2)M^2]^{-1}$
α' = first thermal coefficient of resistance
β = $(\gamma-1)M^2\alpha$
β' = second thermal coefficient of resistance
β_1 = $\omega\tau/b^2$
γ = ratio of specific heats
γ_1 = $b^2(1+j\beta)$
δ = $\left[1 - \frac{b^2}{s^2}\frac{R_{\text{support}}}{R_a}\right]\mu_1$
η = T_a/T_t
μ = viscosity
μ_1 = $\left[\frac{1+j\beta_1}{j\beta_1}\right]\left[\frac{\tanh b}{b} - \frac{\tanh\gamma_1}{\gamma_1}\right]\Big/\left[1 - \frac{\tanh\gamma_1}{\gamma_1}\right]$
ρ = density
τ = $mc\ell^2/\pi d^2 k_w$
τ_{wr} = $(T_a - T_t)/T_t$

Subscripts and Superscripts

a = evaluated at the adiabatic wire temperature
w = evaluated at wire temperature
$(\,)'$ = fluctuating quantity
$\bar{(\,)}$ = mean quantity
$\langle\,\rangle$ = rms quantity

Introduction

OVER the years, a number of research groups[1-3] have utilized shock tubes to generate flows from low subsonic to high supersonic Mach numbers over various geometry bodies upon which heat-transfer measurements have been made. Knowledge of the flow turbulence level, critical for interpretation of such heat-transfer measurements, has previously been lacking. Turbulence measurements for subsonic compressible Mach number flows in a shock tube are reported here.

At Rensselaer Polytechnic Institute (RPI), basic research utilizing shock-tube facilities is being undertaken to make heat-transfer measurements at temperatures and pressures up to 4000°F and 600 psi, respectively, for use in future gas turbine design. The shock tubes are capable of duplicating full-scale turbine inlet conditions of Mach number, Reynolds number, and total temperature. Cylindrically capped flat plates and flat plates with pressure gradients are used to model the stagnation point and the pressure and suction sides of gas turbine blades and vanes. Heat transfer is measured with thin film painted heat gages.

The effect of freestream turbulence on stagnation point heat transfer has been investigated by a number of persons, both experimentally and analytically.[4-7] Turbulence intensity, length scale, and Reynolds number all affect stagnation point Nusselt number. Turbulence intensity is seen to have

Received Feb. 28, 1984; presented as Paper 84-0631 at the AIAA 13th Aerodynamics Testing Conference, San Diego, Calif., March 5-7, 1984; revision received Nov. 7, 1984.

*Doctoral Student, Aeronautical Engineering, Rensselaer Polytechnic Institute, Troy, N.Y. Member AIAA.

†Associate Professor, Department of Mechanical Engineering, Aeronautical Engineering, and Mechanics. Associate Fellow AIAA.

the greatest effect, although length scale is important, particularly at higher turbulence intensities and Reynolds numbers.

This study has two purposes. The first is to measure flow turbulence levels in the shock-induced flows used for stagnation heat-transfer measurements at RPI. Turbulence intensities and spectra will be measured at several Reynolds numbers for a Mach number characteristic of turbine inlet conditions. The second purpose is to take advantage of the reflected shock technique used to establish the low Mach number, high temperature flows, and make measurements of turbulence amplification across a shock wave.

Amplification of turbulence fluctuations across a shock wave has been investigated theoretically and experimentally. Particular attention has been paid to generation of acoustic waves by the interaction of a shock wave and vortex,[8-12] and between a shock and entropy wave.[13] General linear equations for the generation and transmission of fluctuation modes caused by interaction of plane waves with a shock have been derived by McKenzie and Westphal.[14] Results for disturbances in the form of linear plane waves have been numerically integrated over different frequencies and angles of obliqueness to investigate generation and transmission coefficients across a shock.[15-17] Since vortex stretching is not accounted for, verification of the accuracy of these predictions awaits suitable quantitative experimental data.

Zang et al.[17] indicate four mechanisms whereby turbulence levels may be changed across a shock: 1) refraction of incident turbulence through the shock, 2) generation of turbulence from incident entropy and acoustic fluctuations, 3) focusing of high-frequency turbulence by low-frequency shock distortions, and 4) direct conversion of mean flow energy into turbulence by shock oscillation. Since the flow in the shock tube is initially quiescent, it is postulated that waves from the boundary layer and contact surface impinge on and distort the incident shock, causing unsteady focusing of vorticity. Transmission, generation, and shock oscillation effects are expected to be operative across the reflected shock.

There are few published results of hot-wire measurements in shock tubes; all of which have reported mean flow measurements. The authors are unaware of any measurements of fluctuating quantities. The earliest works[18,19] evaluated the suitability of constant current anemometers for mean velocity and temperature measurement. Later work dealt with the calibration and use of cold wires[20] and constant-temperature hot wires[21] for mean flows. Total temperature profiles were measured with a constant-temperature hot wire behind wedges and cones in a hypersonic shock tunnel.[22]

Theory

The hot-wire anemometer measures flow fluctuations through the variations of heat transfer from a heated filament. Postulating that voltage fluctuations are related to fluctuations in the heat-transfer coefficient h, and the adiabatic mean wire resistance R_a, one can write

$$\frac{e'}{\bar{e}} = A_h \frac{h'}{\bar{h}} + A_a \frac{R_a'}{R_a} \tag{1}$$

Corrections for finite aspect ratio can be included through the technique of Lord[23,24] in the coefficients A_h and A_a. Morkovin[25] has shown that

$$\frac{e'}{\bar{e}} = S_\rho \frac{\rho'}{\bar{\rho}} + S_u \frac{u'}{\bar{u}} + S_{T_t} \frac{T_t'}{\bar{T}_t} \tag{2}$$

where for a constant-temperature anemometer the sensitivity coefficients can be shown to be[26]

$$S_\rho = A_h \frac{\partial(\ell n Nu)}{\partial(\ell n Re)} - A_a K \frac{\partial(\ell n \eta)}{\partial(\ell n Re)} \tag{3}$$

$$S_u = S_\rho + \frac{1}{\alpha}\left\{ A_h \frac{\partial(\ell n Nu)}{\partial(\ell n M)} - K A_a \frac{\partial(\ell n \eta)}{\partial(\ell n M)} \right\} \tag{4}$$

$$S_{T_t} = \frac{1}{2}(S_\rho - S_u) - m_t S_\rho - \frac{K}{2A_w'} - A_h(K - 1 - n_t) \tag{5}$$

Although A_h and A_a are complex, Lord has shown that they can be approximated by their real part with good accuracy.

The sensitivity coefficients vary with wire temperature, and three wires at three temperatures generate three equations of form of Eq. (2). They can be solved simultaneously for $u'/\bar{u}$, $\rho'/\bar{\rho}$, and $T_t'/\bar{T}_t$ at each point in time following methods proposed by Stainback et al.[27]

Under certain conditions (e.g., $M > 1.2$, or high overheat), derivatives of Nussult number and recovery temperature ratio with Mach number are negligible[25,27-29]; in which case Eq. (2) becomes

$$\frac{e'}{\bar{e}} = S_{\rho u} \frac{(\rho u)'}{\overline{\rho u}} + S_{T_t} \frac{T_t'}{\bar{T}_t} \tag{6}$$

where

$$S_{\rho u} = S_\rho$$

Two wires operated at different overheats allow separation of the voltage signals into total temperature and mass flux fluctuations. When instantaneous pressure readings are available, separation into velocity and density fluctuations is possible. When only rms pressure measurements are available, rms density and velocity fluctuations are calculated by

$$\left\langle \frac{\rho'}{\bar{\rho}} \right\rangle^2 = \left[\frac{1}{\alpha + \beta} \right]^2 \left\{ \alpha^2 \left\langle \frac{p'}{\bar{p}} \right\rangle^2 + \beta^2 \left\langle \frac{(\rho u)'}{\overline{\rho u}} \right\rangle^2 + \left\langle \frac{T_t'}{\bar{T}_t} \right\rangle^2 + 2\alpha\beta R_{p,\rho u} \left\langle \frac{p'}{\bar{p}} \right\rangle \left\langle \frac{(\rho u)'}{\overline{\rho u}} \right\rangle - 2\alpha R_{p,T_t} \times \left\langle \frac{p'}{\bar{p}} \right\rangle \left\langle \frac{T_t'}{\bar{T}_t} \right\rangle + 2\beta R_{\rho u, T_t} \left\langle \frac{T_t'}{\bar{T}_t} \right\rangle \left\langle \frac{(\rho u)'}{\overline{\rho u}} \right\rangle \right\} \tag{7}$$

$$\left\langle \frac{u'}{\bar{u}} \right\rangle^2 = \left[\frac{\alpha}{\alpha + \beta} \right]^2 \left\{ \left\langle \frac{(\rho u)'}{\overline{\rho u}} \right\rangle^2 + \left\langle \frac{p'}{\bar{p}} \right\rangle^2 + \frac{1}{\alpha^2} \left\langle \frac{T_t'}{\bar{T}_t} \right\rangle^2 - 2\alpha R_{p,T_t} \left\langle \frac{p'}{\bar{p}} \right\rangle \left\langle \frac{T_t'}{\bar{T}_t} \right\rangle + 2\alpha\beta R_{p,\rho u} \left\langle \frac{(\rho u)'}{\overline{\rho u}} \right\rangle \left\langle \frac{p'}{\bar{p}} \right\rangle - 2\beta R_{p,T_t} \left\langle \frac{T_t'}{\bar{T}_t} \right\rangle \left\langle \frac{(\rho u)'}{\overline{\rho u}} \right\rangle \right\} \tag{8}$$

where the brackets $\langle\ \rangle$ denote rms values. Values for correlation coefficients R_{p,T_t} and $R_{p,\rho u}$ must be known. Because of the additional complication, the pressure fluctuations are typically ignored.

Dynamic finite wire length corrections are accounted for in the coefficients A_h and A_a. Values of calibration parameters τ, a^2/I^2, and s^2/h are calculated from measured values of ℓ, α, and R_0. Handbook or manufacturers' values are used for m, c, k_w, and d. Steady finite aspect ratio effects are accounted for as proposed by Dewey.[30] The method is iterative, although uncomplicated. Corrections for radiation heat transfer, free convection, and wire shape change under load can be shown to be small.[26] Mounting the wire with considerable initial slack greatly decreases wire vibration. Residual voltage fluctuations due to wire vibration can

be filtered out with digital signal processing if the peak is prominent.

Facility and Instrumentation

A shock-tube facility was used in this study. The low-pressure tube was 4 in. in diameter with a 62-ft-long driven section and a 10-ft driver. It is pressure limited at 100 psi. Plastic, rubberized cloth, and aluminum were used as diaphragm materials for different pressure ranges. This facility is shown in Fig. 1.

Initial pressures were measured with Heise gages and mercury manometers. Static pressure on the shock-tube sidewall was measured with piezoelectric transducers and charge amplifiers. The pressure gages were calibrated both statically and dynamically. Gage output was linear with pressure jump over the pressure range covered in the experiments.

The shock Mach number was measured in several ways. The primary measurement was to time the shock speed between two fixed locations. Amplified signals from two piezoelectric crystals were fed into a counter/timer. Shock velocities were also measured by timing response of the pressure gages located at various positions along the shock tube. Previous calibration has shown that the pressure ratio across the incident shock, as predicted from inviscid theory, agrees within 5% of the measured pressure ratio. The experimental pressure ratio can then be used as a third measure of shock Mach number. Only runs where three measurements gave agreement in shock Mach number to within 5% were used. The locations of various transducers and sensors in the shock tube are shown in Fig. 2.

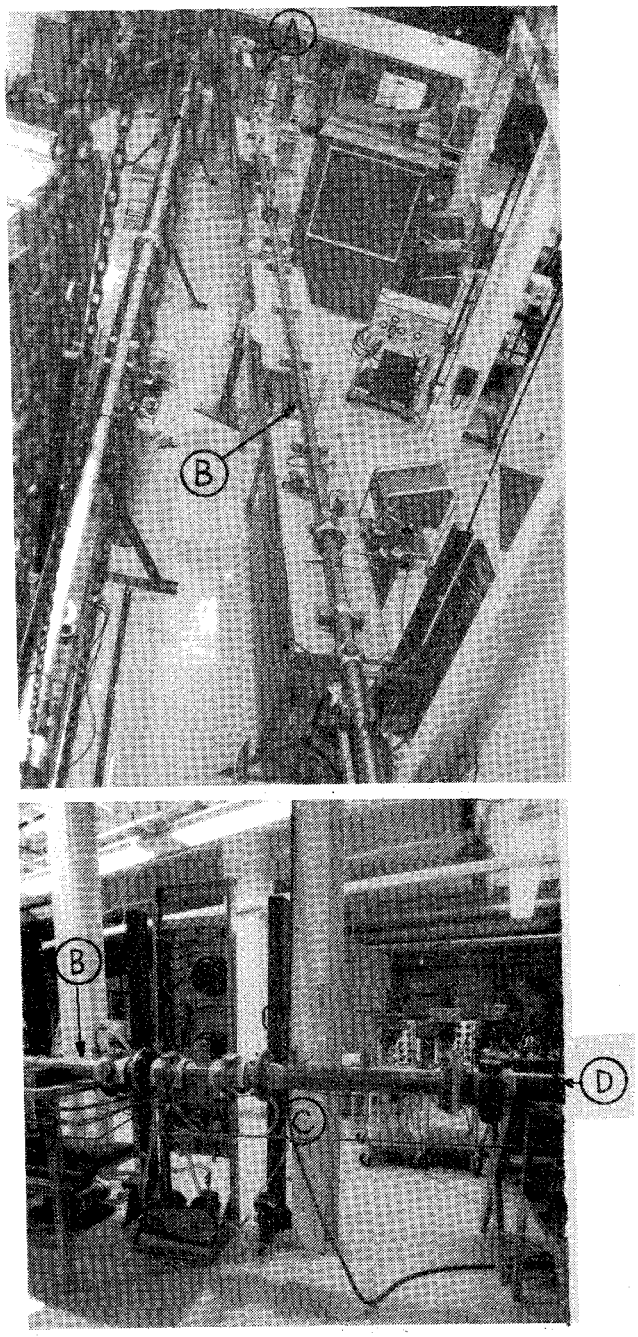

Fig. 1 Test facility, low-pressure shock tube. A: driver, B: driven tube, C: reflecting plate, and D: dump tank.

Voltage traces were photographed from the screens of oscilloscopes. Mean flow data were read directly from the photographs. Fluctuating hot-wire voltage traces were digitized from the photographs for computer processing.

A Thermo Systems Inc. (TSI) model 1051-2 power supply and two model 1050 anemometers were used in this study. Probes were built on TSI 1244 parallel wire probe bodies. Uncoated tungsten wire of 0.00015 in. nominal diameter was used as the sensing elements. The tungsten wire was spot welded to the probe needle tips, with enough slack to follow slightly less than the profile of a quarter-circle between needles.

Tungsten wire oxidizes at about 300°C in air. Consequently, these tests are run in nitrogen. Wire preconditioning, in which the wire was heated above the maximum expected operating temperature in still nitrogen, and the nitrogen test atmosphere, allowed operation up to 400°C. Preconditioning causes a large irreversible reference resistance change. The wire can then be used until this reference resistance changes by more than 0.5%.

The wire resistance vs temperature relation used was

$$R_w = R_0[1+\alpha'(T_w - T_0)+\beta'(T_w - T_0)^2] \tag{9}$$

Values for α' were checked in air and an ice bath. The nominal value was $0.004°C^{-1}$. Calibrated values were tested for α'; the nominal value of $8\times10^{-7}°C^{-2}$ was used for β'.

Wire heat-transfer characteristics are required to calculate wire sensitivities, in particular the logarithmic derivatives of Nu and η with respect to Re and M. Each of these parameters should be calibrated for each wire. Due to limited wire lifetime in the shock tube, this was not possible. All η derivatives were calculated from the curve fit data of Dewey.[30] At fixed M and τ_{wr}, a curve of the form

$$Nu = bRe^n \tag{10}$$

could be fit to the data. For most wires, the exponent n was found to vary with τ_{wr} as

$$n = [0.47(1+3.7\tau_{wr})]\,(n|_{\tau_{wr}=0.3}) \tag{11}$$

The nominal value of n at $\tau_{wr=0.3}$ was found to be approximately 0.35 with some consistency. The logarithmic derivative of Nusselt number with Mach number was taken at zero. This assumption and the use of a nominal slope for $\partial(\ell nNu)/\partial(\ell nRe)$ are expected to be the largest sources of error in this study.

Test Data

The calibration parameter A'_w occurs in the total temperature sensitivity coefficient, S_{T_t}. An accurate determination of A'_w is required to separate mass flux from total temperature fluctuations.

A'_w is obtained in the following manner. The heat balance equation on hot wire, neglecting finite aspect ratio correction, is

$$e^2/R_w = I^2R_w = \pi\ell dh(T_w - T_{rec}) \tag{12}$$

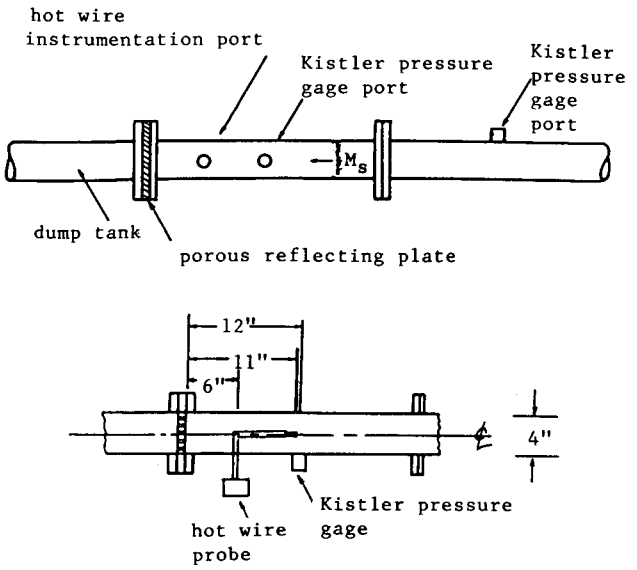

Fig. 2 Instrumentation locations.

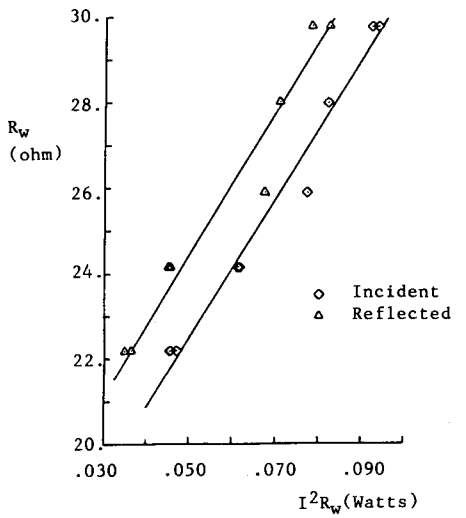

Fig. 3 Wire resistance vs power; incident *Re*/in. = 60,000 and reflected *Re*/in. = 25,000.

Using a first-order wire resistance to wire temperature relation, one finds (assuming constant h) that

$$I^2R_w = C_1R_w + C_2 \tag{13}$$

Data were found to correlate well according to this relationship under conditions of constant Re and M. The calibration parameter can then be evaluated as

$$A'_w = -[1 + (C_1/C_2)R_w] \tag{14}$$

Examples of the data and curve fit used to determine A'_w are shown in Figs. 3 and 4.

Typical response of the Kistler pressure transducers and the hot-wire anemometer to incident and reflected shocks is shown in Figs. 5 and 6. Pressure was increased across each shock wave.

However, anemometer response is somewhat different. A large jump follows the incident shock, with wire vibration quite prominent in the first few microseconds following the incident shock. These strain-gage vibrations rapidly die down. Anemometer output drops across the reflected shock. Output voltage is roughly proportional to the quarter power of mass flux and half power of the difference between wire

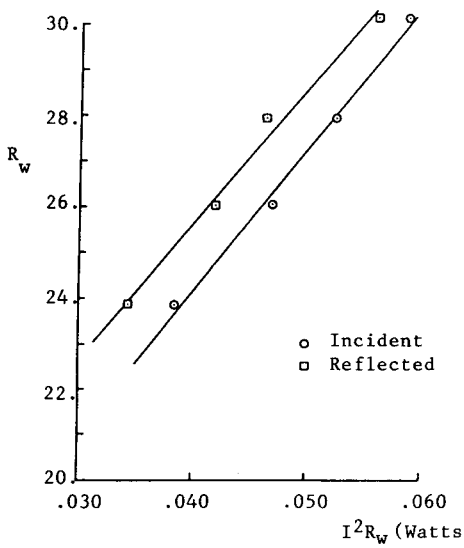

Fig. 4 Wire resistance vs power; incident *Re*/in. = 25,000 and reflected *Re*/in. = 12,000.

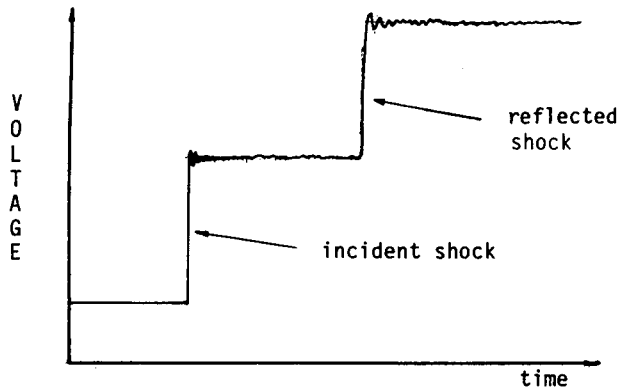

Fig. 5 Typical Kistler pressure gage response to incident and reflected shocks.

and flow recovery temperature. Both mass flux and temperature difference decrease across the reflected shock. Gage vibration is again evident, but of smaller amplitude and shorter duration than behind the incident shock.

Figure 7 shows the output of two pressure gages and two hot wires for a typical run. The characteristic output as described previously can be seen. Figures 8 and 9 show typical amplified hot-wire response output in the incident and reflected regions for one test. Voltage fluctuations in the incident region are clearly smaller than in the reflected region. Fluctuations in anemometer output can be compared between the two traces, and are matched relatively easily, particularly in the reflected region. The trace variations appear to be random, indicating small or no wire vibrations, at least after the first 100 ms in the reflected region. Fourier transforms of the anemometer voltage signals were taken, and showed no particular peak easily related to wire vibration.

Measurements of rms wall static pressure were made to estimate the error in the zero-pressure fluctuation assumption. Fluctuating pressure-gage output had a large component due to gage vibration. Measurements of rms pressure can be taken only as upper bounds. In both incident and reflected regions, rms pressure levels varied from 0.5 to 2.3%. Correlation coefficients R_{p,T_t} and $R_{p,\rho u}$ are unknown.

Frequency content of the hot-wire signal is shown in Fig. 10. The Nyquist frequency corresponds to a normalized frequency of 0.5, and a physical frequency of 100 kHz. The signal is essential broadband from 1 to 50 kHz, dropping abruptly above 50 kHz. Turbulence intensities reported

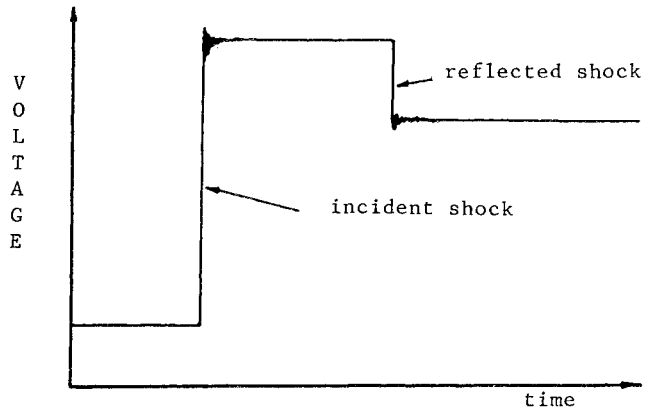

Fig. 6 Typical hot-wire anemometer response to incident and reflected shocks.

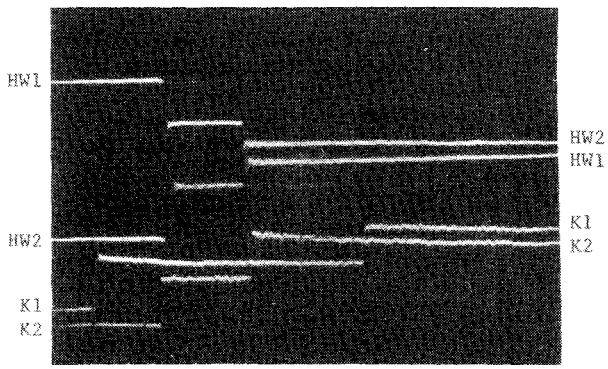

Fig. 7 Typical output of hot-wire anemometer and Kistler pressure gage. Test conditions (reflected region): $M=0.15$, $Re/\text{in.}=85{,}000$, sweep = 1.0 ms/cm, $T_t=720°\text{R}$, $T_{w1}=325°\text{C}$, and $T_{w2}=250°\text{C}$.

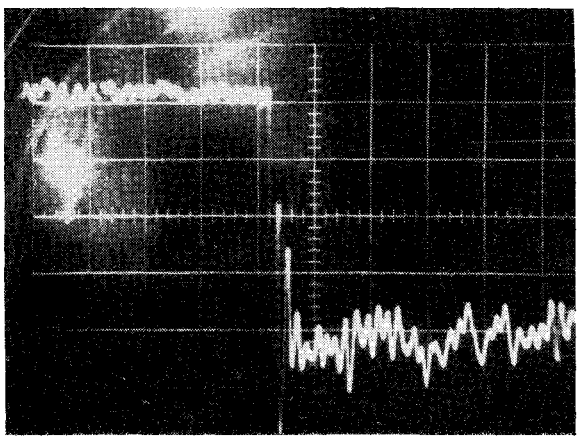

Fig. 8 Amplified hot-wire output, wire 1. Gain, 50 mV/cm; sweep, 200 μs/cm.

herein are for frequencies greater than 1 kHz; the lower limit due to the roughly 1-ms test time.

Results

Digitized data from anemometer output, such as shown previously, mean output data obtained from information such as recorded in Fig. 7, and calibration data of the anemometer sensors were computer-processed to obtain the turbulence intensities. Root-mean-square mass flux and total temperature fluctuation intensities in the incident region are shown in Fig. 11. Temperature fluctuations are two to three times lower than mass flux fluctuations. Mass flux fluctuations are typically 1.1% at $Re/\text{in.}=20{,}000$, decreasing to 0.6% at $Re/\text{in.}=60{,}000$, rising to 1.6% at $Re/\text{in.}=100{,}000$,

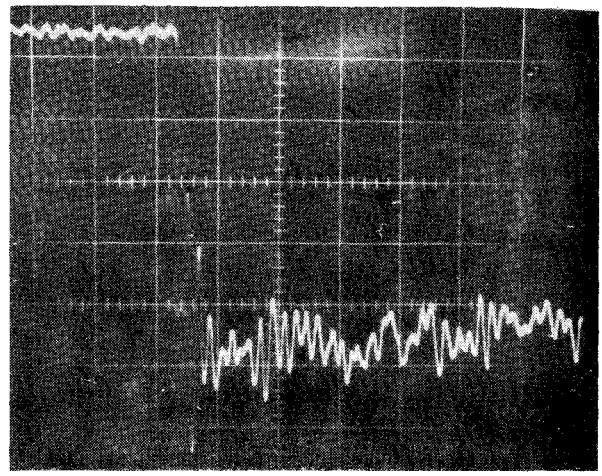

Fig. 9 Amplified hot-wire output, wire 2. Gain, 50 mV/cm; sweep, 200 μs/cm.

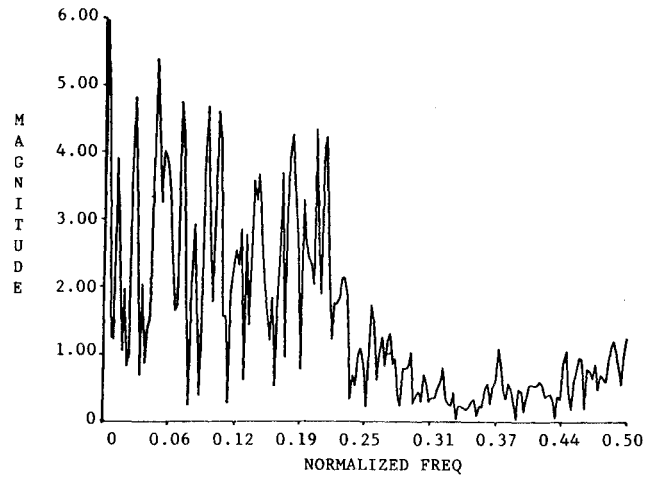

Fig. 10 Amplitude vs frequency of a wire output voltage.

and falling slightly to 1.5% at $Re/\text{in.}=170{,}000$. There is some scatter at the highest and lowest Reynolds numbers in mass flux intensity. Total temperature intensity results are more consistent.

Similar data are shown in Fig. 12 for the reflected region, which is of the greater interest since this is the region in which the heat-transfer experiments are conducted. Again, mass flux fluctuations are two to three times total temperature fluctuations. The same trend of intensities with Reynolds number is evident; i.e., an initial decrease from 5.5 to 2.5% at $Re/\text{in.}=12{,}000$-$25{,}000$, then an increase back to 5.0% at $Re/\text{in.}$ of 40,000, with a decrease to 3.5% at $Re/\text{in.}=82{,}000$. More scatter occurs at the lowest Reynolds number. Comparison with the incident data shows that the highest incident intensities correspond to the highest reflected intensities, and in both incident and reflected regions high mass flux intensities are two to three times larger than temperature fluctuation intensities. The correlation coefficient $R_{\rho u, T_t}$ was between 0.85 and 1.0 in 80% of the runs, but was as low as 0.29 in one case.

Mass flux and total temperature rms values can be used to determine rms density and velocity fluctuations using Eqs. (7) and (8). A knowledge of pressure fluctuations, however, is required. Flow disturbances due to the size of a fast response pressure transducer precluded its placement near the hot wires. The usual assumption that $\langle p' \rangle = 0$ was used in this study. Results for density and velocity fluctuations for the incident and reflected regions are shown in Figs. 13 and

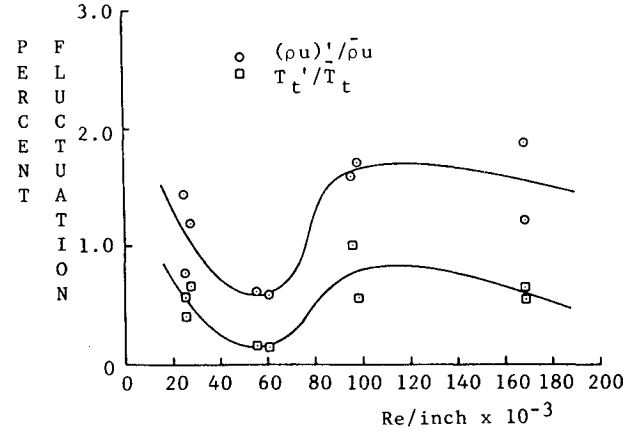

Fig. 11 Mass flux and total temperature fluctuations vs Reynolds number per inch (incident region).

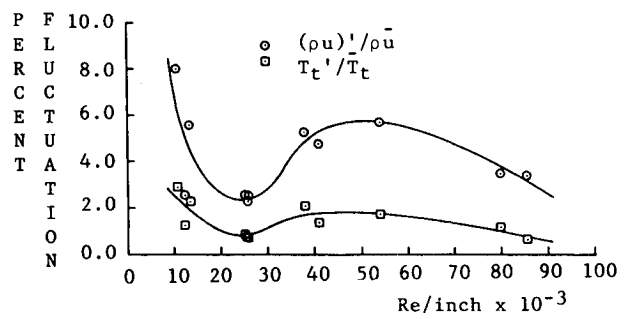

Fig. 12 Mass flux and total temperature fluctuations vs Reynolds number per inch (reflected region).

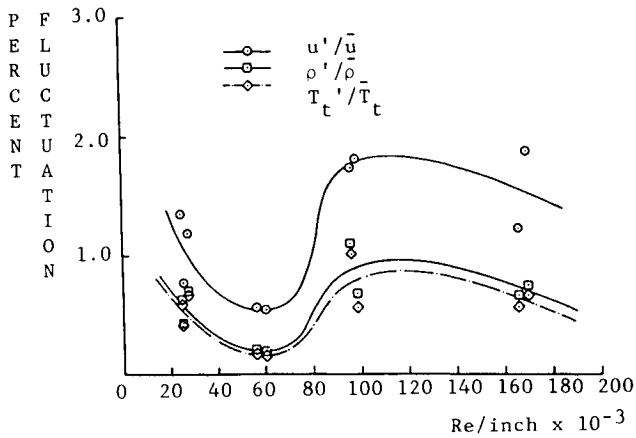

Fig. 13 Velocity, density, and total temperature fluctuations vs Reynolds number per inch (incident region).

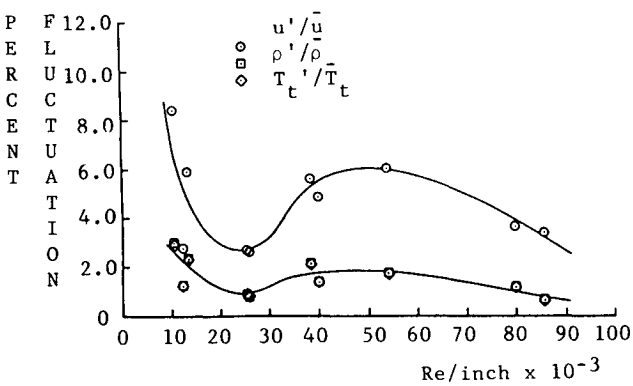

Fig. 14 Velocity, density, and total temperature fluctuations vs Reynolds number per inch (reflected region).

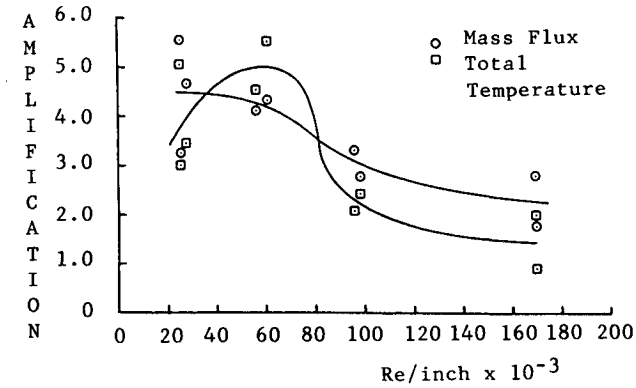

Fig. 15 Amplification of turbulence ratio of rms mass flux and total temperature fluctuations across the reflected shock.

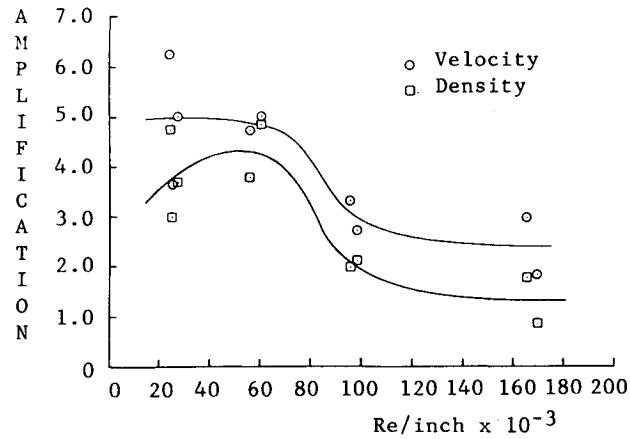

Fig. 16 Amplification of turbulence ratio of rms velocity and density fluctuations across the reflected shock.

14, respectively. In both regions velocity fluctuations essentially follow mass flux fluctuations, although somewhat higher in the reflected region. Density fluctuations are slightly higher than total temperature fluctuations in the incident region but, for all practical purposes, are equal to the temperature fluctuations in the reflected region.

Discussion of Results

The initiation of the incident shock which establishes the test conditions of the experiments is generated by rupturing the diaphragm with a pneumatically driven cutter which initially separates the high-pressure driven gas from the test gas in the driven tube. For the Reynolds number range covered in these experiments, the diaphragm material was soft plastic for the lowest reflected *Re*/in. of 12,000, cloth-reinforced rubber sheeting for *Re*/in. = 25,000, and aluminum sheeting for all higher *Re* tests. Previous testing has shown that the opening characteristics of the diaphragm depend on the pressure ratio existing across it prior to rupture. In particular, higher pressure ratios result in a more rapid and complete opening of the diaphragm. The diaphragm opening process can affect the shock formation and contact surface, both of which could alter flow turbulence level. It is seen that intensity levels are lower at the higher Reynolds number when aluminum diaphragms are used. There is a general consistency of data between incident and reflected regions. Considering these factors, it is thought that diaphragm opening characteristics might play a strong role in the flow turbulence level. However, more extensive tests with a diaphragm over a range of pressures would be needed before any strong conclusions could be drawn. Nevertheless, the overall turbulence levels are small and, thus, do not preclude the use of shock-tube facilities as experimental tools in gathering heat-transfer data.

A question of considerable recent interest deals with amplification of turbulence across a shock wave. Measurements in the incident and reflected regions are used to determine such amplification. Amplification of mass flux and total temperature fluctuations across the reflected shock decreases with increasing incident Reynolds number, as seen in Fig. 15. Amplification of velocity and density fluctuations is shown in Fig. 16.

Conclusions

Measurements have been taken of turbulence levels in compressible subsonic shock-induced flows. Measurements were made in a low-pressure shock tube in the incident and reflected regions of the wave system with a double-wire hot-wire anemometer system. Pressures were monitored by quartz pressure transducers. Fluctuating hot-wire output voltages were recorded, digitized, filtered, corrected for finite wire aspect ratio effects, and analyzed to predict mass flux and total temperature intensities. The assumption of constant pressure allowed the mass flux intensity to be separated into velocity and density fluctuations.

Mass flux fluctuations are between 0.6 and 1.6% in the incident region, and between 2 and 6% in the reflected region. Total temperature fluctuations are consistently two to three times lower than mass flux fluctuations.

Separation of velocity and density fluctuations from mass flux and total temperature fluctuations requires knowledge of the pressure fluctuation. A zero-pressure fluctuation assumption is reasonable considering the low magnitude of the upper bounds on $\langle p' \rangle$.

Velocity and density fluctuations follow those of mass flux and total temperature, respectively. Turbulence quantities are amplified across the reflected shock by a factor which generally decreases with Reynolds number in the range of this investigation. Mass flux and velocity fluctuations are amplified more than total temperature and density.

Acknowledgment

This study was jointly sponsored by the National Science Foundation and NASA Lewis Research Center.

References

[1]Hertzberg, A., Smith, W. E., Glick, H. S., and Squire, W., "Modification of the Shock Tube for the Generation of Hypersonic Flow," Cornell Aeronautical Lab., Rept. AD-789-A-2, AEDC TN 55-15, AD 63559, 1955.

[2]Nagamatsu, H. T., Geiger, R. E., and Sheer, R. E. Jr., "Hypersonic Shock Tunnel," *ARS Journal*, Vol. 29, 1959, p. 332.

[3]Schultz, D. L., Jones, T. V., Oldfied, J. L., Ainsworth, R. W., and Daniels, L. A., "The Measurement of Heat Transfer Rates to Film Cooled External Surfaces and the Interval Passages of Turbomachine Components under Transient Conditions Using Thin Film Gages," Engineering Laboratory, Oxford, England, 1976.

[4]Kestin, J., "The Effect of Freestream Turbulence on Heat Transfer Rates," *Advances in Heat Transfer*, Vol. 3, 1966, pp. 1-32.

[5]Traci, R. M. and Wilcox, D. C., "Freestream Turbulence Effects on Stagnation Point Heat Transfer," *AIAA Journal*, Vol. 13, July 1975, pp. 890-896.

[6]Sunden, B., "A Theoretical Investigation of the Effect of Freestream Turbulence on Skin Friction and Heat Transfer for a Bluff Body," *International Journal on Heat and Mass Transfer*, Vol. 22, 1979, pp. 1125-1135.

[7]Kestin, J. and Wood, R., "The Influence of Turbulence on Mass Transfer from Cylinders," *Journal on Heat Transfer*, Vol. 93C, Nov. 1971, pp. 321-327.

[8]Kovasznay, L.S.G., "Interaction of a Shock Wave and Turbulence," *Proceedings of Heat Transfer and Fluid Mechanics Institute*, 1955.

[9]Ribner, H. S., "Shock Turbulence Interaction and the Generation of Noise," NACA Rept. 1233, 1955.

[10]Weeks, T. M. and Dosanjh, D. S., "Sound Generation by Shock Vortex Interaction," *AIAA Journal*, Vol. 5, April 1967, pp. 660-669.

[11]Ting, L., "Transmission of Singularities Through a Shock Wave and the Sound Generation," *The Physics of Fluids*, Vol. 17, Aug. 1974, pp. 1518-1526.

[12]Dosanjh, D. S. and Weeks, T. M., "Interaction of a Starting Vortex as Well as a Vortex Sheet with a Traveling Shock Wave," *AIAA Journal*, Vol. 3, Feb. 1965, pp. 216-223.

[13]Chang, C-T., "Interaction of a Plane Shock and Oblique Plane Disturbance with Special Reference to Entropy Waves," *Journal of the Aeronautical Sciences*, Vol. 24, Sept. 1957, pp. 675-682.

[14]McKenzie, J. F. and Westphal, K. O., "Interaction of Linear Waves with Oblique Shock Waves," *The Physics of Fluids*, Vol. 11, Nov. 1968, pp. 2350-2362.

[15]Anyiwo, J. C. and Bushnell, D. M., "Turbulence Amplification in Shock Wave Boundary Layer Interaction," *AIAA Journal*, Vol. 20, July 1982, pp. 893-899.

[16]Zang, T. A., Hussaini, M. Y., and Bushnell, D. M., "Numerical Computations of Turbulence Amplifications in Shock Wave Interactions," AIAA Paper 82-0293, Jan. 1982.

[17]Zang, T. A., Hussaini, M. Y., and Bushnell, D. M., "Numerical Computations of Turbulence Amplification in Shock Wave Interactions," ICASE Rept. 83-10, NASA Langley Research Center, Hampton, VA, April 28, 1983.

[18]Dosanjh, D. S., "Use of Hot Wire Anemometer in Shock Tube Investigation," NACA TN 3163, Dec. 1954.

[19]Datar, S. G., "Temperature Response of a Hot Wire Anemometer to Shock and Rarefaction Waves," University of Toronto Insitute of Aeronautics, Toronto, Canada, TN 28, June 1959.

[20]Christiansen, W. H., "Development and Calibration of a Cold Wire Probe for Use in Shock Tubes," Guggenheim Aeronautical Laboratory, California Institute of Technology, Pasadena, CA, Memo. 62, July 1, 1961.

[21]Guy, B., "Gas Velocity Measurements in a Shock Tube with a Hot Wire Anemometer," *Journal of Physics E: Scientific Instruments*, Vol. 4, 1971, pp. 961-965.

[22]Todisco, A. and Pallone, A. J., "Near Wake Flow Field Measurements," *AIAA Journal*, Vol. 3, Nov. 1965, pp. 2075-2080.

[23]Lord, R. G., "Hot Wire Probe End Loss Corrections in Low Density Flows," *Journal of Physics E: Scientific Instruments*, Vol. 7, 1974, pp. 56-60.

[24]Lord, R. G., "The Dynamic Behavior of Hot Wire Anemometers with Conduction End Losses," *Journal of Physics E: Scientific Instruments*, Vol. 14, 1981, pp. 573-578.

[25]Morkovin, M. V., "Hot Wire Anemometry in Compressible Flows," AGARDograph 24, 1955.

[26]Trolier, J. W., "Turbulence Measurements in Shock Induced Flows," Ph.D. Thesis, Rensselaer Polytechnic Institute, Troy, N.Y., May 1984.

[27]Stainback, P. C., Johnson, C. B., and Basnett, C. B., "Preliminary Measurements of Velocity, Density, and Total Temperature Fluctuations in Compressible Subsonic Flows," AIAA Paper 83-0384, Jan. 1983.

[28]Kovasznay, L.S.G., "Turbulence in Supersonic Flow," *Journal of the Aerospace Sciences*, Vol. 20, Oct. 1953, pp. 653-682.

[29]Horstman, C. C. and Rose, W. C., "Hot Wire Anemometry in Transonic Flow," *AIAA Journal*, Vol. 15, March 1977, pp. 395-401.

[30]Dewey, C. F., "Hot Wire Measurements in Low Reynolds Number Hypersonic Flows," *ARS Journal*, Vol. 28, Dec. 1961, pp. 1709-1718.